Survey of Gravitationally Lensed Objects in HSC Imaging (SuGOHI) VII. Discovery and confirmation of three strongly lensed quasars

Jaelani, A.T.; Rusu, C.E.; Kayo, I.; More, A.; Sonnenfeld, A.; Silverman, J.D.; ... ; Inoue, K.T.

Survey of Gravitationally lensed Objects in HSC Imaging (SuGOHI) – VII. Discovery and Confirmation of Three Strongly Lensed Quasars[†]

Anton T. Jaelani[1,2][★], Cristian E. Rusu[3], Issha Kayo[4], Anupreeta More[5,6], Alessandro Sonnenfeld[5,7], John D. Silverman[5,8], Malte Schramm[3], Timo Anguita[9,10], Naohisa Inada[11], Daichi Kondo[12], Paul L. Schechter[13], Khee-Gan Lee[5], Masamune Oguri[5,14,15], James H. H. Chan[16], Kenneth C. Wong[5], and Kaiki T. Inoue[1]

[1]*Department of Physics, Kindai University, 3-4-1 Kowakae, Higashi-Osaka, Osaka 577-8502, Japan*
[2]*Astronomy Research Division and Bosscha Observatory, FMIPA, Institut Teknologi Bandung, Jl. Ganesha 10, Bandung 40132, Indonesia*
[3]*National Astronomical Observatory of Japan, 2-21-1 Osawa, Mitaka, Tokyo 181-0015, Japan*
[4]*Department of Liberal Arts, Tokyo University of Technology, Ota-ku, Tokyo 144-8650, Japan*
[5]*Kavli Institute for the Physics and Mathematics of the Universe (WPI), UTIAS, The University of Tokyo, Kashiwa, Chiba 277-8583, Japan*
[8]*Department of Astronomy, The University of Tokyo, 7-3-1 Hongo, Bunkyo-ku, Tokyo 113-0033, Japan*
[9]*Departamento de Ciencias Fisicas, Universidad Andres Bello, Fernandez Concha 700, Las Condes, Santiago, Chile*
[10]*Millennium Institute of Astrophysics (MAS), Nuncio MonseÃśor Sotero Sanz 100, Providencia, Santiago, Chile*
[11]*Department of Physics, Nara National College of Technology, Yamatokohriyama, Nara 639-1080, Japan*
[12]*School of Computer Science, Tokyo University of Technology, 1404-1 Katakuramachi, Hachioji City, Tokyo 192-0982, Japan*
[13]*MIT Kavli Institute 37-664G, 77 Massachusetts Avenue, Cambridge, MA 02139-4307, USA*
[14]*Department of Physics, The University of Tokyo, 7-3-1 Hongo, Bunkyo-ku, Tokyo 113-0033, Japan*
[15]*Research Center for the Early Universe, The University of Tokyo, 7-3-1 Hongo, Bunkyo-ku, Tokyo 113-0033, Japan*
[16]*Laboratoire d'Astrophysique, Ecole Polytechnique Fédérale de Lausanne (EPFL), Observatoire de Sauverny, CH-1290 Versoix, Switzerland*
[†]*This paper includes data gathered with the 6.5 meter Magellan Telescopes located at Las Campanas Observatory, Chile.*

ABSTRACT

We present spectroscopic confirmation of three new two-image gravitationally lensed quasars, compiled from existing strong lens and X-ray catalogs. Images of HSC J091843.27–022007.5 show a red galaxy with two blue point sources at either side, separated by 2.26 arcsec. This system has a source and a lens redshifts $z_{\rm s}$ = 0.804 and z_{ℓ} = 0.459, respectively, as obtained by our follow-up spectroscopic data. CXCO J100201.50+020330.0 shows two point sources separated by 0.85 arcsec on either side of an early-type galaxy. The follow-up spectroscopic data confirm the fainter quasar has the same redshift with the brighter quasar from the SDSS fiber spectrum at $z_{\rm s}$ = 2.016. The deflecting foreground galaxy is a typical early-type galaxy at a redshift of z_{ℓ} = 0.439. SDSS J135944.21+012809.8 has two point sources with quasar spectra at the same redshift $z_{\rm s}$ = 1.096, separated by 1.05 arcsec, and fits to the HSC images confirm the presence of a galaxy between these. These discoveries demonstrate the power of the Hyper Suprime-Cam Subaru Strategic Program (HSC-SSP)'s deep imaging and wide sky coverage. Combined with existing X-ray source catalogues and follow-up spectroscopy, the HSC-SSP provides us unique opportunities to find multiple-image quasars lensed by a foreground galaxy.

Key words: gravitational lensing: strong – methods: observational.

1 INTRODUCTION

Over the four decades since the discovery of the first gravitationally lensed quasar (Walsh et al. 1979), these systems have proven to be invaluable probes for both astrophysics

★ E-mail: anton@phys.kindai.ac.jp

and cosmology (e.g., Claeskens & Surdej 2002; Treu & Marshall 2016). Astrophysical applications range from intermediate redshifts, with the measurement of extragalactic extinction curves (e.g., Falco et al. 1999; Østman et al. 2008), the direct detection of dark matter substructures (e.g., Dalal & Kochanek 2002; Vegetti et al. 2012), constraints on Warm Dark Matter (WDM; e.g., Inoue et al. 2015), and the calibration of the stellar mass fundamental plane (e.g., Schechter et al. 2014), to high redshifts, with elucidating the structure of quasar accretion disks (e.g., Yonehara et al. 1998; Poindexter et al. 2008), their broad line regions (e.g., Sluse et al. 2012; Fian et al. 2018), and the coevolution of supermassive black holes with their hosts galaxies (e.g., Peng et al. 2006; Ding et al. 2017). In cosmology, statistically complete samples of lensed quasars are used to set constraints on dark energy (e.g., Oguri et al. 2008, 2012), and lensed quasars with measured time delays are used to infer the Hubble-Lemaître constant independent from other probes (e.g., Suyu et al. 2010; Bonvin et al. 2017; Wong et al. 2020).

While these applications are broad, they all require distinct sample selection criteria, such that studies utilising lensed quasars are limited at present by the small number of ~ 220 known systems.[1] Nonetheless, the numbers have increased considerably over the past decade and a half, due to the availability of large-scale, deep multi-band optical imaging surveys such as the Sloan Digital Sky Survey (SDSS, York et al. 2000), and more recently the Panoramic Survey Telescope and Rapid Response System (Pan-STARRS, Chambers et al. 2016), the Dark Energy Survey (DES, Abbott et al. 2018), the Hyper Suprime-Cam Subaru Strategic Program (HSC-SSP, Aihara et al. 2018a), and the Dark Energy Spectroscopic Instrument (DESI) Legacy Imaging Surveys (Dey et al. 2019). Various data mining techniques have been employed to isolate the intrinsically rare lensed quasars (Oguri & Marshall 2010) among the vast amounts of possible contaminants. These include selecting from a parent spectroscopic catalogue and applying morphological and colour criteria (e.g., Oguri et al. 2006a), using machine learning techniques on both catalogue and pixel data (e.g., Agnello et al. 2015), or engaging citizen science volunteers to visually inspect large numbers of images (e.g., Sonnenfeld et al. 2020a). Ultimately however, to convincingly confirm a system as a lensed quasar requires extensive follow-up spectroscopy campaigns, which is why publishing lists of candidates is common in the literature (e.g., Chan et al. 2020a; Rusu et al. 2019).

In this paper, we present the spectroscopic confirmation of three new strongly lensed quasars compiled from previous catalogs applied to the HSC-SSP footprint: HSC J091843.27–022007.5, CXCO J100201.50+020330.0, and SDSS J135944.21+012809.8 (hereafter J0918, J1002, and J1359) at (RA Dec.) = (139.6803, −2.3354), (150.5063, +2.0582), and (209.9342, +1.4693), respectively. Our paper is organised as follows. Section 2 briefly illustrates the candidate-compilation process. In Section 3, we describe the imaging analysis. We present the results of the spectroscopic follow-up observations of the systems in Section 4. In Section 5, we present the mass modelling of the systems, and we

---

[1] An up-to-date database is maintained at https://web1.ast.cam.ac.uk/ioa/research/lensedquasars/.

conclude in Section 6. Throughout this paper, we adopt a concordance cosmology with $\Omega_m = 0.27$, $\Omega_\Lambda = 0.73$, $H_0 = 73$ km s^{-1} Mpc^{-1}. All quoted magnitudes are on the AB system, position angles are measured East of North, and uncertainties are 1σ and are assumed to be Gaussian.

2   LENSED QUASAR CANDIDATE COMPILATION

The lens candidates we report here are not the result of a single systematic search. Instead, we compiled candidates from three different methods employed by several of the authors: looking for close companion object in the Chandra catalog of X-ray selected objects (Evans et al. 2010), carried out by co-author Anupreeta More, re-inspection of the Sloan Digital Sky Survey Quasar Lens Search (SQLS, e.g., Oguri et al. 2006b; Inada et al. 2012) catalog, conducted by co-author Issha Kayo, and further examination of the Survey of Gravitationally-lensed Objects in HSC Imaging (SuGOHI, Sonnenfeld et al. 2018, 2020b; Wong et al. 2018; Chan et al. 2020b; Jaelani et al. 2020). In total, we selected 5 candidates, two from the first two methods each, and three from SuGOHI, for conducting follow-up spectroscopic observations. Details of each candidate are described in the next sections.

3   IMAGING

In this work, we use photometric data from the HSC Wide S18A internal data release of the HSC survey (Aihara et al. 2019). The HSC Survey is an ongoing imaging survey, expected to cover about 1,400 deg^2 in five bands (g, r, i, z and y) down to $r \sim 26$ with the Hyper Suprime-Cam (Aihara et al. 2018b; Miyazaki et al. 2018; Komiyama et al. 2018; Kawanomoto et al. 2018; Furusawa et al. 2018), using a wide-field (1.7-degree diameter) optical camera installed on the 8.2-m Subaru Telescope. The data are processed with hscPipe, which is derived from the Vera C. Rubin Observatory's Legacy Survey of Space and Time pipeline (Axelrod et al. 2010; Jurić et al. 2017; Ivezić et al. 2008, 2019).

We model and analyse the multiband HSC imaging data for the lens systems using GALFIT (Peng et al. 2002). For each system, we measure relative positions of the fainter quasar and the lens galaxy with respect to the brighter quasar, by fitting a model composed of a point source for each quasar image and a Sérsic profile convolved with the point spread function (PSF) for the lens galaxy. The PSF models are generated using the PSF Picker tool Aihara et al. (see details in 2018c, 2019) for all of the HSC bands. Magnitudes of each component, derived from the fits, are given in Table 1.

In Figure 1, we show the HSC multiband imaging cutouts as well as the PSF-subtracted images, revealing the lens galaxies. In general, the lenses are brighter in y band and the quasars in g band, as expected from their red and blue colours, respectively. We show an additional image of J1002 from data archive of the Hubble Space Telescope (HST) Advanced Camera for Surveys (ACS) Wide Field Channel (WFC), part of the Cosmic Evolution Survey (COSMOS, Scoville et al. 2007a,b; Koekemoer et al. 2007) with 5σ de-
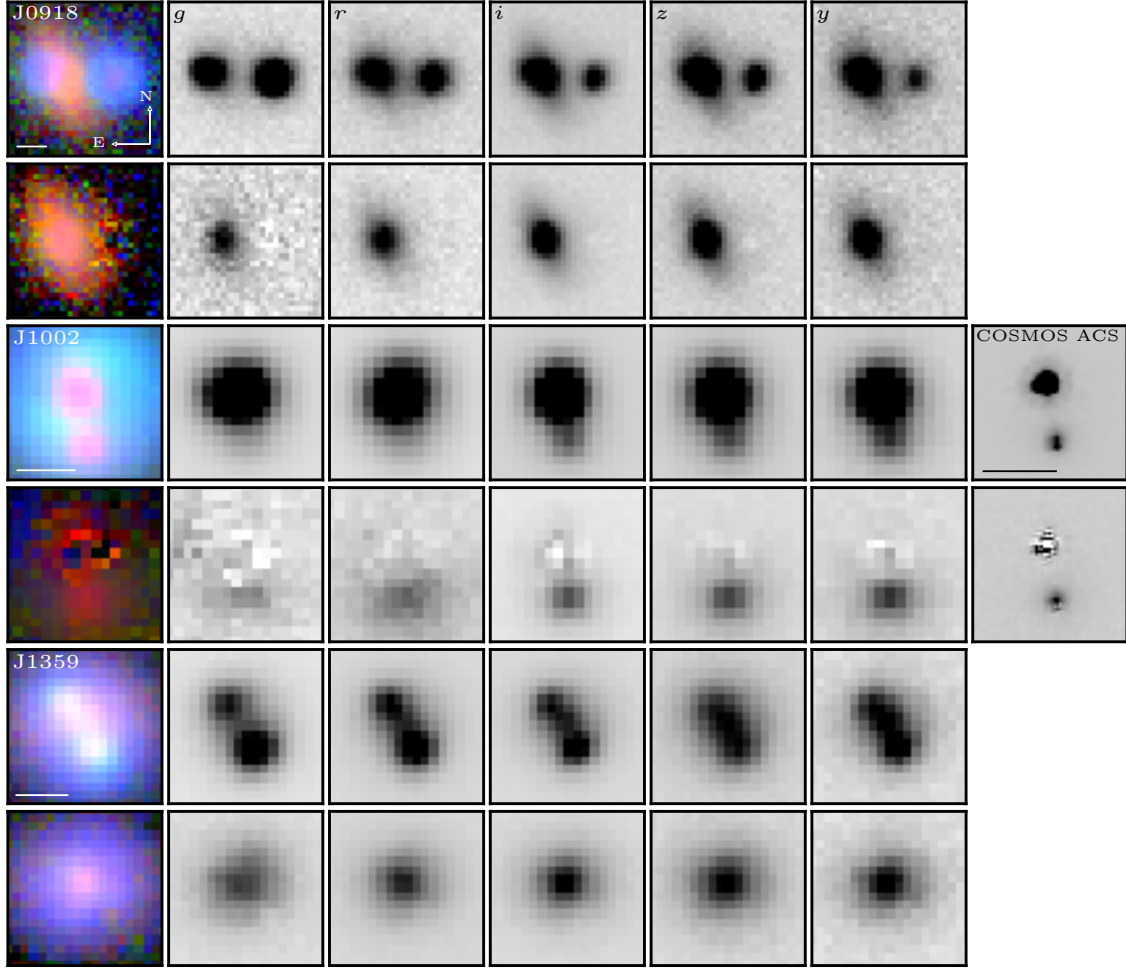
Figure 1. HSC *gri* composite and multiband images of the three lensed quasars. Additionally, the COSMOS ACS F814W image for J1002 is shown. The photometric bands are denoted in the upper left corner. Corresponding point source-substracted images based on the `GALFIT` best-fit in each band are shown below the data. The size of each image of J0918, J1002, and J1359 are 5.54, 2.87, and 3.19 arcsec, respectively. North is up and East is left. Scale bars of 1 arcsec are displayed in the bottom left corner.

Table 1. Properties of three confirmed lensed quasars. The redshifts of lens and source are obtained from our follow-up spectra. The relative astrometry in arcsec, and the magnitudes of the brighter (A), the fainter (B) quasar image and the lens galaxy (G) are obtained by fitting the HSC images using `GALFIT`. The HSC image quality, in terms of the "seeing" FWHM in arcsec, is also quoted. A tentative result $z_\ell = 0.35$ for J1359.

| System [z_ℓ, z_s]		ΔRA	ΔDec.	g	r	i	z	y
	A	0.00	0.00	20.57 ± 0.09	20.50 ± 0.09	20.73 ± 0.11	20.22 ± 0.05	20.46 ± 0.11
J0918 [0.459, 0.804]	B	−2.25 ± 0.02	0.22 ± 0.02	21.34 ± 0.13	21.24 ± 0.08	21.44 ± 0.13	20.99 ± 0.10	21.21 ± 0.06
	G	−1.67 ± 0.04	0.04 ± 0.03	22.12 ± 0.07	20.24 ± 0.06	19.36 ± 0.04	18.99 ± 0.07	18.78 ± 0.07
Seeing				0.82	1.01	0.77	0.74	0.86
	A	0.00	0.00	18.97 ± 0.23	18.63 ± 0.20	18.40 ± 0.26	18.32 ± 0.18	18.29 ± 0.29
J1002 [0.439, 2.016]	B	0.14 ± 0.03	−0.84 ± 0.02	22.88 ± 0.17	21.79 ± 0.16	21.68 ± 0.20	21.52 ± 0.13	21.37 ± 0.13
	G	0.13 ± 0.03	−0.74 ± 0.04	23.84 ± 0.15	22.23 ± 0.14	21.14 ± 0.11	20.83 ± 0.12	20.71 ± 0.11
Seeing				0.78	0.92	0.59	0.62	0.61
	A	0.00	0.00	21.03 ± 0.19	20.58 ± 0.12	20.58 ± 0.17	20.63 ± 0.11	20.43 ± 0.11
J1359 [− , 1.096]	B	−0.54 ± 0.02	0.90 ± 0.02	21.80 ± 0.13	21.33 ± 0.16	21.31 ± 0.18	21.35 ± 0.12	21.08 ± 0.16
	G	−0.23 ± 0.03	0.55 ± 0.04	21.43 ± 0.05	20.22 ± 0.13	19.75 ± 0.08	19.31 ± 0.10	19.08 ± 0.12
Seeing				0.70	0.61	0.57	0.66	0.55
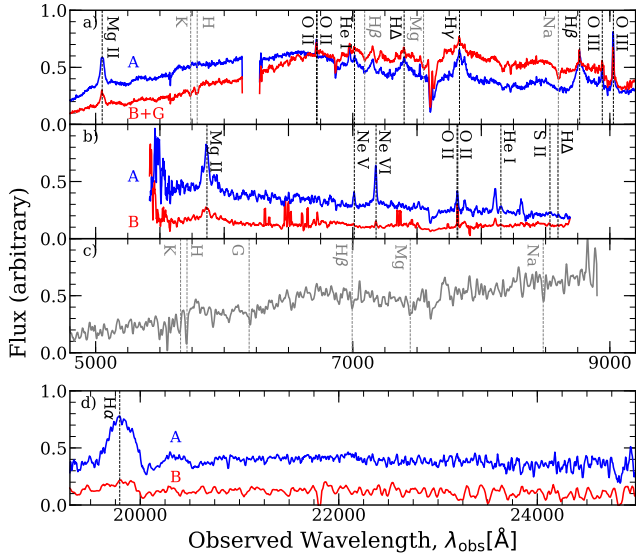
Figure 2. 1D spectra of J0918 (panel a), J1002 (panel c, d), and J1359 (panel b). Panel b shows only the "red part" of the LRIS spectra, with range 5500 - 8500Å. The blue and red lines show the two components, demonstrating that they are a nearly identical quasar spectrum, and the grey line in panel c is the lens galaxy spectra. Emission and absorption lines are marked by black and grey dashed vertical lines, respectively.

tection limits for point sources of 27.2 AB magnitude in F814W, hereafter COSMOS ACS.

4   SPECTROSCOPIC CONFIRMATION

Here, we describe our follow-up spectroscopic results for each lens system. All observations were processed using standard techniques within `IRAF`, and flux-calibrated using observations of spectrophotometric standards.

4.1   J0918

J0918 system was first discovered by Sonnenfeld et al. (2020b) as part of the citizen science project SPACEWARPS (Marshall et al. 2016; More et al. 2016) using over 442 deg^2 of data from the HSC survey. A volunteer identified two blue point-like feature and a putative galaxy in between. A spectrum was obtained with the Inamori Magellan Areal Camera and Spectrograph (IMACS; Dressler et al. 2011) on the Baade 6.5-m telescope on 2019 April 1 and 2 (DirectorâĂŹs Discretionary Time, PI: P. Schechter) using f/2 camera, 0.9 arcsec wide-slit, and 200 mm^{-1} grism.

The 1D spectra of the two point sources correspond to a nearly identical quasar spectrum at $z_s = 0.804 \pm 0.001$, based on Mg II, O II, He I, Hδ, Hγ, Hβ, O III lines. The blended absorption lines of the lens galaxy with the fainter quasar B can be seen clearly based on Ca K, Ca H, Hβ, Mg b, and Na D, yielding a lens galaxy redshift of $z_\ell = 0.459$ (see panel a in Figure 2). Together with the presence of a red galaxy in HSC images, the spectra confirm J0918 as a strongly lensed quasar, with image separation 2.26 arcsec.
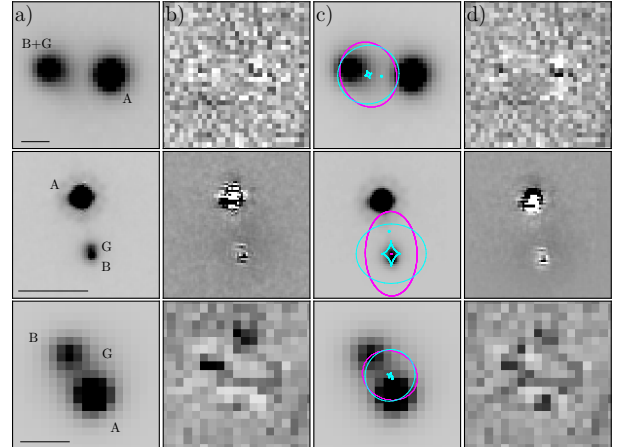

Figure 3. Panel a: Model images generated from `GALFIT` using a PSF for the source images and a Sérsic model convolved with the PSF for the lens galaxy, showing the positions of the doubly-lensed quasar images (A, B) and the early-type lens galaxy (G) for each system (from top to bottom, J0918, J1002 and J1359, respectively). The black solid bar at the bottom left of the panel shows a scale of 1 arcsec. Panel b: `GALFIT` model-subtracted residual images. Panel c: Model images generated from lens mass modelling of the lens system, where the source is assumed to be a point source. Magenta and cyan lines indicate critical curves and caustic, respectively. The true source positions are shown by cyan dots. Panel d: The residual image obtained by subtracting the model from the data.

4.2   J1002

This candidate was chosen from the Chandra catalog of X-ray selected objects (Evans et al. 2010). These X-ray selected AGN sources were inspected in the optical imaging search for the presence of any close companions (e.g., Liu et al. 2013). This system was first detected in the Sloan Digital Sky Survey (SDSS) as SDSS J100201.51+020329.4 as a quasar with spectroscopic redshift of 2.016. Furthermore, this system also has CFHTLS optical and near-infrared imaging, and the COSMOS-Very Large Array (1.4 GHz) imaging in the radio shows a detection. However, the spatial resolution and sensitivity of these data are not enough to resolve this system. The HSC images of J1002, however, unambiguously reveal the presence of two sources with image separation ≈ 0.8 arcsec. This is an excellent example of HSC images being ideal for finding small separation lenses. In the COSMOS ACS F814W imaging, we further detect emission from a third object, which is acting as the lens galaxy (see Figures 1 and 3). With `GALFIT`, we measure magnitudes of A = 18.52, B = 22.03, and G = 21.38 mag.

A near-infrared *K*-band (22,000Å) spectrum was obtained with the Infrared Camera and Spectrograph (IRCS; Tokunaga et al. 1998; Kobayashi et al. 2000) at Subaru Telescope using a setup of 0.45 × 18.0 arcsec slit, 52 milliarcsec mode, *R* ~ 400, and *K*-grism that covers the 19,300 - 24,800Å range, assisted with the Adaptive Optics system AO188 (Hayano et al. 2008, 2010), on 2012 November 27 (o12438, PI: M. Schramm). The 1D spectra of the two sources show the same broad emission line of Hα at $z_s = 2.016 \pm 0.003$. The results suggest that the fainter quasar is highly likely to be at the same redshift as the brighter quasar (see panel d of Figure 2).

Table 2. Best-fit model parameters with 1σ errors from MCMC: SIE velocity dispersion σ_{SIE}, ellipticity e_{SIE}, position angle $\theta_{e_{SIE}}$, reduced χ^2, degree of freedom N_{DOF}, total source magnification μ_{tot}, time delay between the two lensed images Δt_{AB}, Einstein radius θ_{Ein}, and enclosed mass M_{Ein}.

Lens Parameter	J0918	J1002	J1359
σ_{SIE} (km s^{-1})	319 ± 5	155 ± 3	173 ± 2
e_{SIE}	0.16 ± 0.04	0.39 ± 0.03	0.14 ± 0.04
$\theta_{e_{SIE}}$ (deg)	20 ± 5	1 ± 4	67 ± 4
χ^2_{red}	1.36	2.27	1.43
N_{DOF}	1284	2847	789
μ_{tot}	4.3 ± 1.8	4.9 ± 2.1	10.7 ± 3.1
Δt_{AB}, days	-141.3 ± 5.7	-18.7 ± 4.6	-5.6 ± 1.8
θ_{Ein}, arcsec	1.11 ± 0.04	0.48 ± 0.03	0.53 ± 0.01
M_{Ein}, $10^{11}h^{-1}M_{\odot}$	6.40 ± 0.40	0.63 ± 0.08	0.75 ± 0.04

We also carried out deep optical spectroscopy to obtain the redshift of the lens galaxy. We used the Faint Object Camera and Spectrograph (FOCAS; Kashikawa et al. 2002) at Subaru Telescope on 2014 October 23 (o14500, PI: A. More). The observations were made with 1 arcsec long-slit mode, a 300R grating, and an SO58 order-cut filter, giving a spectral coverage of 5800-10000Å with a dispersion of 1.34Å pixel^{-1}. We detect absorption lines from the lens galaxy based on Ca K, Ca H, G-band, Hβ, Mg b, and Na D at $z_{\ell} = 0.439 \pm 0.001$ (see panel c of Figure 2).

4.3 J1359

J1359 system was listed as a likely lens candidate by the Sloan Digital Sky Survey Quasar Lens Search (SQLS, e.g., Oguri et al. 2006b; Inada et al. 2012), however follow-up observations had not been performed due to the small separation (≤ 1 arcsec). We reinspected the SQLS candidate lists using HSC images and re-graded this system as a highly likely candidate. We can clearly observe an extended object (galaxy) between two point sources with quite similar colours (see Figure 1). The quasar was first detected in the SDSS as SDSS J135944.21+012809.8 and has a spectroscopic redshift of 1.096. This system was including as a part of program to confirm dual quasars i.e., physical pairs (Silverman et al. submitted).

We performed spectroscopic follow-up using the dual beam Low Resolution Imaging Spectrometer (LRIS, Oke et al. 1995; Steidel et al. 2004) at the Keck 1 telescope on 2019 January 10 as a backup target during the COSMOS Lyα Mapping And Tomography Observations (CLAMATO) Survey (Lee et al. 2018, U095, PI White). We exposed for 600s in the blue and 590s in the red using the 1 arcsec width long-slit, the 5600Å dichroic, the 600 ℓ mm^{-1} blue grism ($\lambda_{blaze} = 4000$Å), and the 400 ℓ mm^{-1} red grating ($\lambda_{blaze} = 8500$Å). In panel b of Figure 2, we can see separated spectra of the brighter and the fainter quasar, both at $z_s = 1.096 \pm 0.001$ from the identification of several emission lines, Mg II, Ne V, Ne VI, O II, He I, S II, and HΔ, in the red spectra. Unfortunately, we cannot extract the lens galaxy information in the blue spectra due to bad seeing. We find a tentative hint of the 4000Å break feature, which corresponds to redshift $z_{\ell} \approx 0.35$. This is also consistent with our rough estimation of the lens redshift, based on the HSC colours.

5 LENSING PROPERTIES

We used the publicly available lens modelling software `glafic` (Oguri 2010) to model the lensing configuration of the three systems. In order to explore the parameter posteriors, we ran a custom code that combines `glafic` and the `emcee` (Foreman-Mackey et al. 2013) to perform Markov Chain Monte Carlo (MCMC) sampling. With the exception of J1002, where we fitted the COSMOS data, we used the flux information in image pixels (within 7.56, 2.25, and 5.88 arcsec of J0918, J1002, and J1359, respectively) of the lens galaxies and the quasar images in the HSC g band image, which is less contaminated from the lens light, as constraints for the lens mass model. We also masked out pixels did not contribute either to the lens and the sources light from lens model fitting.

Light from the lens galaxy and the unresolved source quasars is modelled with a seven-parameter elliptical Sérsic profile and a three-parameter PSF profile, respectively. We used the best-fitting parameters from `GALFIT` as initial parameters input to `glafic` to model the lens galaxy G. For the source, we let every parameter of the PSF profile vary: magnitude and as well as positions x_s, y_s. We consider a singular isothermal ellipsoid (SIE), with surface density given by $\kappa = \theta_{Ein}/\left(2\sqrt{\tilde{x}^2 + \tilde{y}^2/(1-e)^2}\right)$ where $(\tilde{x}, \tilde{y})$ are the coordinates relative to the lens center along the semi-major and semi-minor axes of the elliptical mass distribution, for the lens mass model. The mass distribution is optimized in the image plane by minimizing χ^2 the flux information between the observed and lens model image. The inferred angular Einstein radius and enclosed mass is defined by

$$\theta_{Ein} = 4\pi \left(\frac{\sigma_{SIE}}{c}\right)^2 \frac{D_{\ell s}}{D_s} \tag{1}$$

and

$$M_{Ein} = \pi \Sigma_{cr}(\theta_{Ein}D_{\ell})^2 \tag{2}$$

with $\Sigma_{cr} = c^2 D_s/(4\pi G D_{\ell} D_{\ell s})$ in terms of angular diameter distance to the source D_s, to the lens D_{ℓ}, between the observer and the source $D_{\ell s}$, with gravitational constant G, and the speed of light c. The results of lens modelling are summarised in Table 2. Note for J1359 we used an estimated lens redshift $z_{\ell} = 0.35$ for the lens mass model.

6 CONCLUSIONS

We have presented the spectroscopic confirmation of three new doubly lensed quasars, compiled from distinct catalogs. The HSC images of J0918 and J1359 reveal two quasar images on either side of lensing source, separated by 2.26 and 1.05 arcsec, respectively, and a close companion for J1002. COSMOS ACS image shows two resolved quasar images and a putative lens galaxy for J1002. Spectra confirm that each system is a lensing system with $z_s = 0.804$, 2.016, and $z_{\ell} = 0.459$, 0.439, for J0918 and J1002, respectively. J1359 has two quasar spectra at $z_s = 1.096$ with similar features and the lens spectrum cannot be extracted due to poor seeing during observation.

We fit SIE lens models to the lenses and infer the Einstein radius and enclosed mass. J1002 and J1359 have velocity dispersion $\sigma_{SIE} = 155$ and 173 km s^{-1} corresponding to

enclosed mass within θ_{Ein} of $M_{\mathrm{Ein}} = 0.63 \times 10^{11}$ and 0.75×10^{11} $h^{-1} M_{\odot}$, respectively. Hence, these systems provide the opportunity to study galaxies from the lower end of the mass function compared to the typical galaxies that have been studied with gravitational lensing so far.

The discovery of these lenses shows us the importance of reanalysis or re-inspection of previous lens search catalogues, by comparing to ongoing or upcoming imaging surveys of superior quality. We have shown that the unique combination of deep, wide imaging, high pixel resolution and good seeing conditions of the HSC data make possible to discover small separation lenses as part of the ongoing SuGOHI search.

REFERENCES

Abbott T. M. C., et al., 2018, ApJS, 239, 18
Agnello A., Kelly B. C., Treu T., Marshall P. J., 2015, MNRAS, 448, 1446
Aihara H., et al., 2018a, PASJ, 70, S4
Aihara H., et al., 2018b, PASJ, 70, S4
Aihara H., et al., 2018c, PASJ, 70, S8
Aihara H., et al., 2019, PASJ, 71, 114
Axelrod T., Kantor J., Lupton R. H., Pierfederici F., 2010, in Proc. SPIE. p. 774015, doi:10.1117/12.857297
Bonvin V., et al., 2017, MNRAS, 465, 4914
Chambers K. C., et al., 2016, arXiv e-prints, p. arXiv:1612.05560
Chan J. H. H., et al., 2020a, A&A, 636, A87
Chan J. H. H., et al., 2020b, A&A, 636, A87
Claeskens J.-F., Surdej J., 2002, A&ARv, 10, 263
Dalal N., Kochanek C. S., 2002, ApJ, 572, 25
Dey A., et al., 2019, AJ, 157, 168
Ding X., et al., 2017, MNRAS, 472, 90
Dressler A., et al., 2011, PASP, 123, 288
Evans I. N., et al., 2010, ApJS, 189, 37
Falco E. E., et al., 1999, ApJ, 523, 617
Fian C., Guerras E., Mediavilla E., Jiménez-Vicente J., Muñoz J. A., Falco E. E., Motta V., Hanslmeier A., 2018, ApJ, 859, 50
Foreman-Mackey D., Hogg D. W., Lang D., Goodman J., 2013, PASP, 125, 306
Furusawa H., et al., 2018, PASJ, 70, S3
Hayano Y., et al., 2008, in Hubin N., Max C. E., Wizinowich P. L., eds, Vol. 7015, Adaptive Optics Systems. SPIE, pp 255 – 262, doi:10.1117/12.789992, https://doi.org/10.1117/12.789992
Hayano Y., et al., 2010, in Ellerbroek B. L., Hart M., Hubin N., Wizinowich P. L., eds, Vol. 7736, Adaptive Optics Systems II. SPIE, pp 260 – 267, doi:10.1117/12.857567, https://doi.org/10.1117/12.857567
Inada N., et al., 2012, AJ, 143, 119
Inoue K. T., Takahashi R., Takahashi T., Ishiyama T., 2015, MNRAS, 448, 2704
Ivezić Z., et al., 2008, Serbian Astronomical Journal, 176, 1
Ivezić Ž., et al., 2019, ApJ, 873, 111
Jaelani A. T., et al., 2020, MNRAS, 495, 1291
Jurić M., et al., 2017, in Lorente N. P. F., Shortridge K., Wayth R., eds, Astronomical Society of the Pacific Conference Series Vol. 512, Astronomical Data Analysis Software and Systems XXV. p. 279 (arXiv:1512.07914)
Kashikawa N., et al., 2002, PASJ, 54, 819
Kawanomoto S., et al., 2018, PASJ, 70, 66
Kobayashi N., et al., 2000, in Iye M., Moorwood A. F. M., eds, Vol. 4008, Optical and IR Telescope Instrumentation and Detectors. SPIE, pp 1056 – 1066, doi:10.1117/12.395423, https://doi.org/10.1117/12.395423
Koekemoer A. M., et al., 2007, ApJS, 172, 196
Komiyama Y., et al., 2018, PASJ, 70, S2
Lee K.-G., et al., 2018, ApJS, 237, 31

Liu X., Civano F., Shen Y., Green P., Greene J. E., Strauss M. A., 2013, ApJ, 762, 110

Marshall P. J., et al., 2016, MNRAS, 455, 1171

Miyazaki S., et al., 2018, PASJ, 70, S1

More A., et al., 2016, MNRAS, 455, 1191

Oguri M., 2010, PASJ, 62, 1017

Oguri M., Marshall P. J., 2010, MNRAS, 405, 2579

Oguri M., et al., 2006a, AJ, 132, 999

Oguri M., et al., 2006b, AJ, 132, 999

Oguri M., et al., 2008, AJ, 135, 512

Oguri M., et al., 2012, AJ, 143, 120

Oke J. B., et al., 1995, PASP, 107, 375

Østman L., Goobar A., Mörtsell E., 2008, A&A, 485, 403

Peng C. Y., Ho L. C., Impey C. D., Rix H.-W., 2002, AJ, 124, 266

Peng C. Y., Impey C. D., Rix H.-W., Kochanek C. S., Keeton C. R., Falco E. E., Lehár J., McLeod B. A., 2006, ApJ, 649, 616

Poindexter S., Morgan N., Kochanek C. S., 2008, ApJ, 673, 34

Rusu C. E., Berghea C. T., Fassnacht C. D., More A., Seman E., Nelson G. J., Chen G. C. F., 2019, MNRAS, 486, 4987

Schechter P. L., Pooley D., Blackburne J. A., Wambsganss J., 2014, ApJ, 793, 96

Scoville N., et al., 2007a, ApJS, 172, 1

Scoville N., et al., 2007b, ApJS, 172, 38

Sluse D., Hutsemékers D., Courbin F., Meylan G., Wambsganss J., 2012, A&A, 544, A62

Sonnenfeld A., et al., 2018, PASJ, 70, S29

Sonnenfeld A., et al., 2020a, arXiv e-prints, p. arXiv:2004.00634

Sonnenfeld A., et al., 2020b, arXiv e-prints, p. arXiv:2004.00634

Steidel C. C., Shapley A. E., Pettini M., Adelberger K. L., Erb D. K., Reddy N. A., Hunt M. P., 2004, ApJ, 604, 534

Suyu S. H., Marshall P. J., Auger M. W., Hilbert S., Blandford R. D., Koopmans L. V. E., Fassnacht C. D., Treu T., 2010, ApJ, 711, 201

Tokunaga A. T., et al., 1998, in Fowler A. M., ed., Vol. 3354, Infrared Astronomical Instrumentation. SPIE, pp 512 – 524, doi:10.1117/12.317277, https://doi.org/10.1117/12.317277

Treu T., Marshall P. J., 2016, A&ARv, 24, 11

Vegetti S., Lagattuta D. J., McKean J. P., Auger M. W., Fassnacht C. D., Koopmans L. V. E., 2012, Nature, 481, 341

Walsh D., Carswell R. F., Weymann R. J., 1979, Nature, 279, 381

Wong K. C., et al., 2018, ApJ, 867, 107

Wong K. C., et al., 2020, MNRAS, in press

Yonehara A., Mineshige S., Manmoto T., Fukue J., Umemura M., Turner E. L., 1998, ApJ, 501, L41

York D. G., et al., 2000, AJ, 120, 1579

APPENDIX A: REJECTED CANDIDATES

By using the same instrument setup for observing J0918 spectra, we observed two other candidates HSC J113957.93−001010.8 and HSC J120755.44−010438.5 (see Figure A1), which we convincingly reject. The first candidate was made up of four blue components in a quad-like configuration, with odd flux ratios. The close pair should have been brighter and the quadrilateral made by the four images has two opposite sides that are twice as big as the other pair of opposite sides. The spectrum of the two brightest components showed ionized knots with Hβ, O III and Hα which indicate a bunch of star forming regions likely associated to a galaxy at $z \sim 0.05$. The spectrum of second candidate likewise showed narrow Hβ and O III at $z = 0.37$.
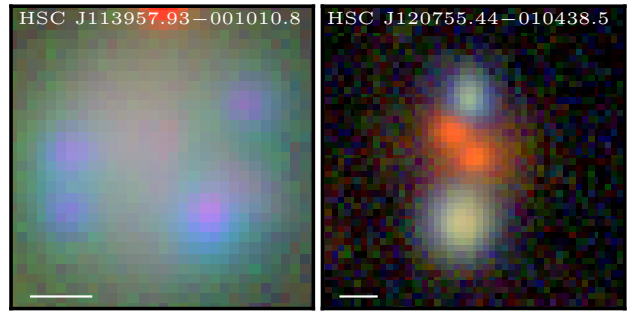

Figure A1. HSC *gri* composite images of the the two rejected candidates. Scale bars of 1 arcsec are displayed in the bottom left corner.

This paper has been typeset from a TeX/LaTeX file prepared by the author.